

# Functional Analysis of Orai1 Concatemers Supports a Hexameric Stoichiometry for the CRAC Channel

Michelle Yen,<sup>1,2</sup> Ludmila A. Lokteva,<sup>1</sup> and Richard S. Lewis<sup>1,2,\*</sup>

<sup>1</sup>Department of Molecular and Cellular Physiology and <sup>2</sup>Graduate Program in Immunology, Stanford University School of Medicine, Stanford, California

**ABSTRACT** Store-operated  $\text{Ca}^{2+}$  entry occurs through the binding of the endoplasmic reticulum (ER)  $\text{Ca}^{2+}$  sensor STIM1 to Orai1, the pore-forming subunit of the  $\text{Ca}^{2+}$  release-activated  $\text{Ca}^{2+}$  (CRAC) channel. Although the essential steps leading to channel opening have been described, fundamental questions remain, including the functional stoichiometry of the CRAC channel. The crystal structure of *Drosophila* Orai indicates a hexameric stoichiometry, while studies of linked Orai1 concatemers and single-molecule photobleaching suggest that channels assemble as tetramers. We assessed CRAC channel stoichiometry by expressing hexameric concatemers of human Orai1 and comparing in detail their ionic currents to those of native CRAC channels and channels generated from monomeric Orai1 constructs. Cell surface biotinylation results indicated that Orai1 channels in the plasma membrane were assembled from intact hexameric polypeptides and not from truncated protein products. In addition, the L273D mutation depressed channel activity equally regardless of which Orai1 subunit in the concatemer carried the mutation. Thus, functional channels were generated from intact Orai1 hexamers in which all subunits contributed equally. These hexameric Orai1 channels displayed the biophysical fingerprint of native CRAC channels, including the distinguishing characteristics of gating (store-dependent activation,  $\text{Ca}^{2+}$ -dependent inactivation, open probability), permeation (ion selectivity, affinity for  $\text{Ca}^{2+}$  block,  $\text{La}^{3+}$  sensitivity, unitary current magnitude), and pharmacology (enhancement and inhibition by 2-aminoethoxydiphenyl borate). Because permeation characteristics depend strongly on pore geometry, it is unlikely that hexameric and tetrameric pores would display identical  $\text{Ca}^{2+}$  affinity, ion selectivity, and unitary current magnitude. Thus, based on the highly similar pore properties of the hexameric Orai1 concatemer and native CRAC channels, we conclude that the CRAC channel functions as a hexamer of Orai1 subunits.

## INTRODUCTION

Store-operated  $\text{Ca}^{2+}$  entry is a ubiquitous mechanism for  $\text{Ca}^{2+}$  signaling and performs a wide variety of essential functions, including immune cell activation by antigen (1,2). The prototypical store-operated channel is the  $\text{Ca}^{2+}$  release-activated  $\text{Ca}^{2+}$  (CRAC) channel, which is distinguished by a set of biophysical characteristics that includes an extremely high  $\text{Ca}^{2+}$  selectivity and low unitary conductance, rapid feedback inhibition by intracellular  $\text{Ca}^{2+}$ , and an inwardly rectifying current-voltage relationship (2). Much progress has been made in elucidating the mechanism of CRAC channel activation since the discovery of its two critical components, the ER  $\text{Ca}^{2+}$  sensor STIM1 and the plasma membrane pore-forming subunit Orai1 (2,3). Depletion of  $\text{Ca}^{2+}$  from the ER triggers STIM1 oligomerization and accumulation at ER-plasma membrane junctions where

it directly binds to and gates Orai1 (2). However, despite our understanding of the overall mechanism of the store-operated  $\text{Ca}^{2+}$  entry and the molecular domains of STIM1 and Orai1 that underlie activation, some of the most fundamental issues remain poorly understood or controversial. These include the number of Orai1 subunits that assemble to form the CRAC channel (4).

Several lines of evidence support a tetrameric CRAC channel stoichiometry. Tetrameric DNA concatemers of human Orai1 (hOrai1) subunits produce currents with inward rectification and a positive reversal potential similar to those of endogenous CRAC channels or of channels generated from monomeric hOrai1 DNA (5–8). Furthermore, channels made from tetrameric concatemers fail to combine with Orai1 monomers, as inferred from a lack of current inhibition by dominant negative monomeric Orai1 (E106Q) (6), and the absence of fluorescence resonance energy transfer between labeled Orai1 protein tetramers and monomers (5). Fluorescence brightness analysis of labeled hOrai1 (9) as well as single-particle photobleaching studies are also

Submitted April 6, 2016, and accepted for publication September 12, 2016.

\*Correspondence: [rslewis@stanford.edu](mailto:rslewis@stanford.edu)

Editor: Chris Lingle.

<http://dx.doi.org/10.1016/j.bpj.2016.09.020>

© 2016 Biophysical Society.



consistent with a tetrameric stoichiometry. Single channels made from GFP-tagged hOrai1 or *Drosophila* Orai (dOrai) subunits bleach in a stepwise manner, with channels assembled from Orai monomers bleaching mostly in 3–4 steps, while tandem dimers or trimers bleach in two steps, and tandem tetramers in a single step (5,10,11). Evidence also supports the existence of hOrai1 and dOrai dimers in the plasma membrane, which have been proposed to oligomerize into tetramers upon STIM binding (10–12), although this conclusion is somewhat controversial (4,9). On balance, the evidence from electrophysiological and photobleaching studies favors a tetrameric stoichiometry for the active CRAC channel.

The argument for a tetrameric CRAC channel stoichiometry was subsequently challenged by the dOrai crystal structure, which depicts the channel as a hexamer of dOrai subunits (13). Size exclusion chromatography and cross-linking studies of dOrai in HEK293 membranes and in detergent (13), as well as atomic force microscopy of hOrai1 decorated with antibodies (14), further support a hexameric stoichiometry. Importantly, the pore-lining residues in TM1 of the dOrai crystal structure agree with results of previous cysteine-scanning studies of hOrai1 in the open and closed states (15,16). In addition, a constitutively active mutant of dOrai (V174A) was shown to conduct  $\text{Na}^+$  after reconstitution into liposomes, and this was prevented by an inhibitory pore mutation (K163W) or by  $\text{Gd}^{3+}$ , showing that it retains at least some CRAC channel properties. However, subsequent electrophysiological analysis showed that channels made from a hexameric hOrai1 concatemer construct lacked two signature features of native CRAC channels, high  $\text{Ca}^{2+}$  selectivity and  $\text{Ca}^{2+}$ -dependent inactivation (CDI) (17), raising questions about whether Orai1 hexamers accurately replicate the full biophysical fingerprint of the CRAC channel.

In this study we applied an electrophysiological approach to address the open question regarding the stoichiometry of the CRAC channel. We designed a concatenated hexameric hOrai1 construct, confirmed its expression as a functional hexameric channel at the plasma membrane, and characterized its biophysical properties in detail. Our results show that an Orai1 hexamer can produce the characteristic biophysical features of the CRAC channel, including permeation properties that are expected to depend strongly on pore geometry. Based on these results, we conclude that the CRAC channel functions as a hexamer of Orai1 subunits.

## MATERIALS AND METHODS

### DNA constructs

#### *Construction of hexameric Orai1 DNA*

Orai1 DNA (containing a T258C silent mutation to remove the endogenous *HindIII* site) was PCR amplified with subunit-specific primers to append

unique restriction sites followed by a linker. For subunit 1, an *XhoI* site and myc tag were appended to the N-terminus and a *BamHI* site was added to the C-terminus. For subunits 2–6, a cleavable linker consisting of a TEV protease recognition sequence (TRS), myc tag, and a Gly-Ser stretch (ENLYFQGEQKLISEEDLNGGGGGS) was added immediately after the 5' restriction site. All subunits were subcloned into pCR-BLUNT II-TOPO vectors before digestion and ligation into the hexamer backbone (Life Technologies, Carlsbad, CA). In the [Supporting Material](#), primer sequences are listed in [Table S1](#), and [Table S2](#) describes the linkers between Orai1 subunits.

The hexamer backbone was modified from eGFP-N1 (Clontech, Mountain View, CA) to contain the TRS sequence (ENLYFQG) N-terminal to the eGFP (primer set 8). The initial WT hexamer was generated by multiple fragment ligation with the digested backbone (*XhoI/BamHI*) and Orai1 subunit fragments (cut with their unique restriction enzyme pair). For mutant hexamer variants, the desired mutations were introduced via site-directed mutagenesis into specific subunits (carried in TOPO vectors) and then ligated into a hexamer via the appropriate restriction sites to substitute for the corresponding WT subunit.

mCherry-STIM1 (mCh-STIM1) has been described in Wu et al. (18). Orai1-GFP was a gift from Dr. Tao Xu (Chinese Academy of Sciences, Beijing, China) (19). All constructs were verified by DNA sequencing (Sequetech, Mountain View, CA).

### Cell culture and transfection

HEK293-H cells (Gibco/Life Technologies, Carlsbad, CA) were passaged in adherent phase in DMEM-based media containing 10% fetal bovine serum, 2 mM L-alanyl-glutamine, and 100 U/mL penicillin/streptomycin and maintained at 37°C in 5%  $\text{CO}_2$ . Cells were transfected with Lipofectamine 2000 (Life Technologies) at 37°C according to the manufacturer's protocol. Unless indicated otherwise, we used a 10:1 DNA mass ratio of mCh-STIM1 to Orai1 hexamer-GFP, or a 4:1 mass ratio of mCh-STIM1 to monomeric Orai1-GFP DNA. After 6 h incubation, cells were given fresh media and maintained at 30°C for 2 d before experiments.

### Biotinylation and western blotting

After rinsing with PBS, a 6 cm dish of confluent HEK293 cells expressing monomeric or hexameric Orai1 constructs were biotinylated with 4 mM sulfo-NHS-LC-biotin (Pierce, Rockford, IL) in PBS for 30 min at 20–22°C. After biotinylation, cells were quenched and washed with PBS containing 50 mM Tris (Sigma-Aldrich, St. Louis, MO), then harvested by scraping and pelleted by centrifugation. Cells were lysed by resuspension in ice-cold RIPA buffer containing protease inhibitor cocktail (Pierce). Lysates were cleared by centrifugation and incubated with streptavidin agarose beads for 30 min at 20–22°C, after which the beads were pelleted by centrifugation and washed three times with RIPA buffer. Protein was eluted by incubation with 4× lithium dodecyl sulfate sample buffer containing 250 mM DTT (Life Technologies) for 5 min at 95°C.

Proteins were resolved on 3–8% Tris-acetate polyacrylamide gels (Life Technologies). After electrophoresis, proteins were transferred to PVDF membrane and probed with rabbit  $\alpha$ -Orai1 (Sigma-Aldrich) and mouse  $\alpha$ -MEK1/2 (Cell Signaling, Beverly, MA) primary antibodies, followed by detection with goat  $\alpha$ -rabbit IR680 and goat  $\alpha$ -mouse IR800 secondary antibodies (LI-COR Biosciences, Lincoln, NE). Blots were visualized and analyzed using a LI-COR Odyssey system.

### Solutions

2 mM  $\text{Ca}^{2+}$  Ringer's solution contained 155 mM NaCl, 4.5 mM KCl, 2 mM  $\text{CaCl}_2$ , 1 mM  $\text{MgCl}_2$ , 10 mM D-glucose, and 5 mM HEPES (pH

7.4 with NaOH). The 20 mM  $\text{Ca}^{2+}$  Ringer's was similar to 2 mM  $\text{Ca}^{2+}$  Ringer's but contained 130 mM NaCl and 20 mM  $\text{CaCl}_2$ . For  $\text{Na}^+$ -free 20 mM  $\text{Ca}^{2+}$  Ringer's,  $\text{Na}^+$  was replaced with equimolar NMDG-Cl (pH 7.4 with HCl). Divalent-free Ringer's (DVF) contained 150 mM NaCl, 10 mM HEDTA, 1 mM EDTA, 10 mM TEA-Cl, and 10 mM HEPES (pH 7.4 with NaOH). For noise analysis experiments, MaxChelator (20) was used to calculate the amount of total  $\text{CaCl}_2$  to add to DVF Ringer's to achieve the desired free  $\text{Ca}^{2+}$  concentration, and the resulting  $\text{Ca}^{2+}$  concentrations were measured using a  $\text{Ca}^{2+}$ -sensitive electrode (Thermo Fisher Scientific, Waltham, MA). Recording pipette solution contained: 150 mM Cs aspartate, 8 mM  $\text{MgCl}_2$ , 10 mM EGTA, and 10 mM HEPES (pH 7.2 with CsOH). All chemical reagents were purchased from Sigma-Aldrich.

## Electrophysiology and microscopy

To obtain reliable CRAC channel characteristics in heterologous expression systems, it is essential to ensure a high ratio of STIM1 to Orai1 protein (21–25). CDI is known to be sensitive to the STIM/Orai ratio (21,22,25); therefore, we only analyzed data from cells with a mCherry/GFP fluorescence ratio sufficient to support full CDI in cells expressing mCh-STIM1 and WT Orai1 hexamer-GFP. This corresponded to a STIM1/Orai1 ratio  $>5$ , as determined using a mCherry-GFP calibrator construct (22). mCherry and GFP fluorescence was measured by wide field imaging at the cell equator, using a 200M Axiovert microscope (Zeiss, Oberkochen, Germany) with a  $40\times$  Fluor NA 1.3 objective, Polychrome II monochromator with xenon lamp (TILL Photonics, Gräfelfing, Germany), GFP filter set ( $488 \pm 10$  excitation, 515 dichroic,  $535 \pm 15$  nm emission), mCherry filter set ( $535 \pm 20$  excitation, 565 dichroic,  $660 \pm 25$  nm emission), and an ORCA-ER CCD camera (Hamamatsu, Hamamatsu City, Japan), controlled by MetaMorph software (Molecular Devices, Sunnyvale, CA).

All patch-clamp measurements were performed at 22–24°C using an Axopatch 200 or 200B amplifier (Axon Instruments/Molecular Devices, Sunnyvale, CA), an InstruTECH ITC-16 interface (HEKA Instruments, Holliston, MA), and a Mac Mini computer (Apple, Cupertino, CA). Recording electrodes were fabricated from 100- $\mu\text{L}$  borosilicate glass pipettes (VWR International, Radnor, PA) and had tip resistances of 2–5 M $\Omega$ . After seal formation and break-in,  $I_{\text{CRAC}}$  was induced by passive ER store depletion via EGTA in the patch pipette. To follow the activation time course, voltage commands (100-ms step to  $-100$  mV followed by a ramp to  $+100$  over 100 ms) were delivered to the cell every 5 s from a holding potential of  $+30$  mV. After  $I_{\text{CRAC}}$  reached a stable maximum, current amplitude was measured as the peak current during steps to  $-100$  mV. CDI was evoked by 200-ms hyperpolarizations delivered every 5 s from a holding potential of  $+30$  mV. CDI was quantified by the current at the end of the voltage step relative to the peak current measured 3 ms after the start of the step (23). All whole-cell currents were leak subtracted using 10–100  $\mu\text{M}$   $\text{LaCl}_3$  in 20 mM  $\text{Ca}^{2+}$  Ringer's. Data collection and analysis were performed using a suite of custom Igor Pro (WaveMetrics, Portland, OR) procedures developed in-house.

The relative permeability of  $\text{Cs}^+$  to  $\text{Na}^+$  was calculated according to the Goldman-Hodgkin-Katz equation  $P_{\text{Cs}}/P_{\text{Na}} = [\text{Na}]_o/[\text{Cs}]_i e^{-E_{\text{rev}}F/RT}$ , where  $R$ ,  $T$ , and  $F$  have their usual meanings, and  $E_{\text{rev}}$  is the reversal potential. The noise analysis experimental protocol was adapted from the general method we have described in Prakriya and Lewis (26) with the following changes. Cells were predepleted with 1  $\mu\text{M}$  thapsigargin, and upon break-in cells were continuously held at  $-100$  mV for the duration of the experiment. 200-ms sweeps were collected every 0.25 s, filtered at 2 kHz, and sampled at 5 kHz. Solutions were perfused locally using an electronic valve system attached to an 8-channel perfusion pencil (AutoMate Scientific, Berkeley, CA) which was coupled to a 19-gauge blunt needle and placed near the cell. The system achieved a local exchange time of  $<2$  s.

## Antibody staining and flow cytometry

HEK293 cells were transfected with mCh-STIM1 and hexameric Orai1 concatemer plasmids and maintained as described above for patch-clamp experiments. A quantity of  $1.5 \times 10^6$  cells per sample were incubated with 10  $\mu\text{g}/\text{mL}$  2C1.1 primary monoclonal antibody (gift from Helen McBride, Amgen, Thousand Oaks, CA) in FACS buffer (PBS with 2% FBS) for 45 min at 4°C. Cells were washed once with FACS buffer and resuspended in 3  $\mu\text{g}/\text{mL}$  goat anti-human IgG conjugated to Alexa594 (Life Technologies) for 20 min at 4°C. After an additional wash with FACS buffer, cells were fixed in 2% paraformaldehyde for 10 min at 22–25°C. Cells were washed twice with FACS buffer before analysis on a FACScan flow cytometer (BD, Franklin Lakes, NJ) using the GFP (488 nm excitation, 560 SP splitter,  $525 \pm 25$  nm emission) and Alexa594 channels (561 nm excitation, 600 SP splitter,  $590 \pm 10$  nm emission).

## RESULTS

### A hexameric concatemer of Orai1 DNA produces contiguous and functional hexameric channels

We designed a hexameric hOrai1 concatemer construct (abbreviated hereafter as “6xOrai1”) to address the question of whether hexameric Orai1 channels display the biophysical characteristics of native CRAC channels. Our construct design incorporated several key features. Each hOrai1 subunit was joined to the next by a 24 amino acid linker that included a *myc* epitope tag, a TEV protease recognition sequence (TRS), and a unique restriction enzyme site (Fig. 1 A; see Materials and Methods). We chose a linker length that was longer than the 6-residue linker used in a previous study (17) to avoid changes in channel behavior that can occur when linkers are too short (27,28). The TRS was included to enable cleavage of the linkers after protein synthesis in the event that the linkers did alter channel behavior, while the unique combination of restriction sites surrounding each subunit was designed to facilitate subunit-specific mutagenesis, cloning, and sequencing.

In principle, concatemers should define the protein subunit stoichiometry of the channel as well as enable mutagenesis of specific subunits. However, channels made from concatemeric DNA constructs do not always assemble as intended. For example, truncated proteins generated by proteolysis or incomplete transcription or translation may recombine before transport to the plasma membrane, creating channels of uncertain and variable subunit composition (28–32). For this reason, we conducted several tests to confirm that the channels in the plasma membrane incorporated all six linked hexamer subunits. SDS-PAGE and western analysis of the lysate from HEK293 cells expressing 6xOrai1 showed predominantly a single band near the molecular weight expected from the sequence (239 kDa) with several faint lower MW bands corresponding to the size of Orai1-GFP monomer (Fig. 1 D, lysate lane). Visual inspection of these cells showed that most of the GFP fluorescence localized to intracellular compartments rather than the plasma membrane (Fig. 1 B), raising the possibility that the subpopulation of channels that trafficked successfully

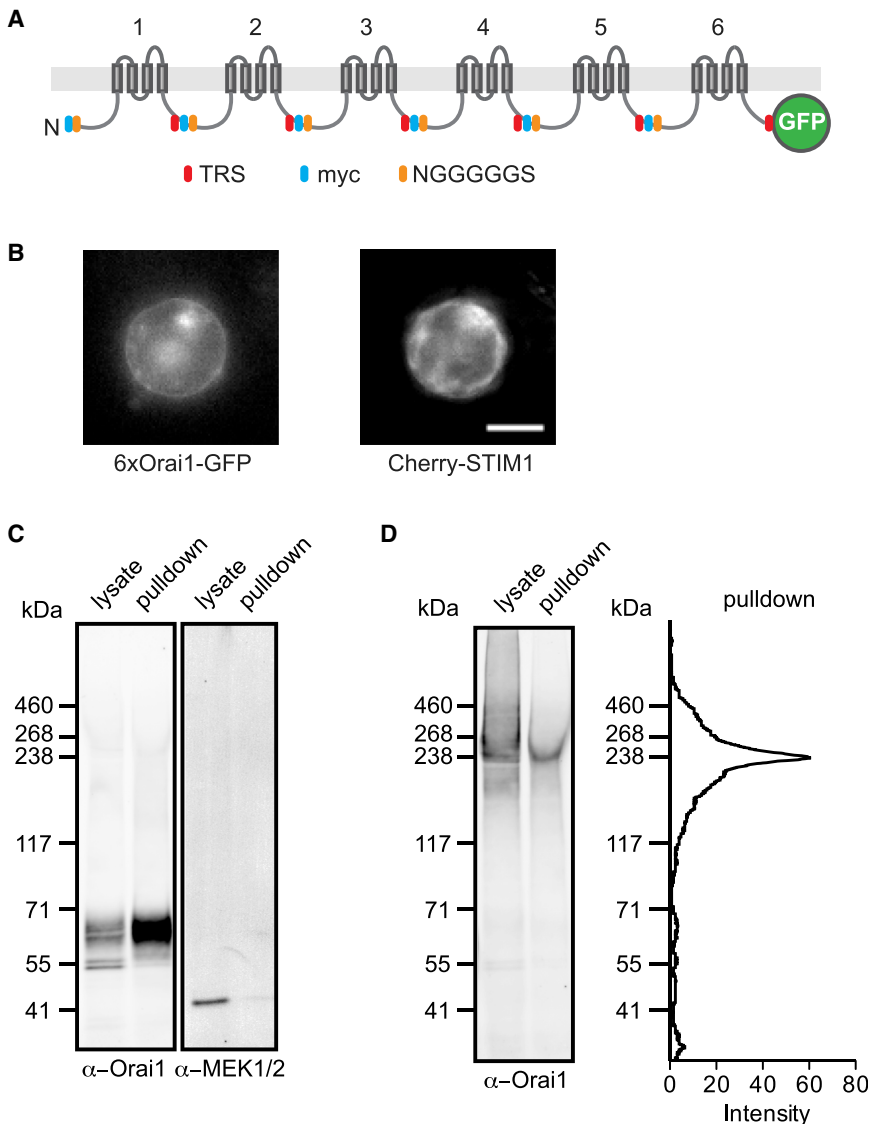


**FIGURE 1** The 6xOrai1 plasmid generates a contiguous hexameric polypeptide at the plasma membrane. (A) The hexameric polypeptide consists of six Orail subunits connected in tandem by 24-residue linkers and GFP fused to the C-terminus. Transmembrane segments are depicted as rectangles. TRS, TEV protease recognition sequence. (B) Fluorescence images of a HEK293 cell coexpressing GFP-labeled 6xOrai1 and mCh-STM1. Scale bar, 4  $\mu$ m. (C) Validation of cell surface biotinylation to isolate plasma membrane proteins. HEK293 cells expressing GFP-tagged 1xOrai1 were labeled with cell-impermeant sulfo-NHS-LC-biotin, and after lysis proteins were pulled down with streptavidin and analyzed by western blot using anti-MEK1/2 and anti-Orail antibodies. Molecular weights of Orail-GFP and MEK1/2 are 64 and 45 kDa, respectively. The integrated fluorescence intensity of Orail was twofold higher in the pull-down lane relative to lysate, whereas in the same sample, MEK1/2 intensity in the pull-down was reduced to 6% relative to lysate, indicating that  $\leq 3\%$  of intracellular protein is carried over into the pull-down fraction. (D) Western analysis of surface-biotinylated HEK293 cells expressing 6xOrai1. The pull-down lane shows a single band near the expected molecular weight of the hexamer of 239 kDa without significant amounts of smaller Orail-derived proteins. Band intensity is quantified in a line scan of the pull-down lane (right). To see this figure in color, go online.

to the plasma membrane might be difficult to detect against a background of intracellular channels. We therefore probed plasma membrane channels specifically by biotinylating the surface proteins of intact cells and isolating them using streptavidin beads. To confirm the plasma membrane specificity of biotinylation, control experiments were performed on cells transfected with monomeric hOrail-GFP plasmid (abbreviated hereafter as "1xOrail"). Western blot analysis of the pull-down fraction showed that Orail protein was retained whereas the endogenous cytosolic protein MEK1/2 was lost, confirming the specificity of the surface biotinylation and pull-down (Fig. 1 C). Importantly, in cells transfected with 6xOrail, the pull-down fraction showed a single protein band at the expected size of full-length hexamer, without significant amounts of smaller Orail proteins that could result from proteolysis or incomplete transcription or translation (Fig. 1 D). Thus, membrane-localized

channels in these cells are assembled from the intact hexameric polypeptide.

These results do not rule out the possibility that some subunits within the hexameric polypeptide are excluded to create channel pores with fewer than six subunits, or that individual channels assemble from multiple polypeptides. For example, tetrameric  $K_V$  channels have been shown to assemble from linked pentamers with the N-terminal subunits being incorporated preferentially (33). To test whether all six subunits of the Orail concatemer are being incorporated equally, we introduced the L273D point mutation into subunits 1, 3, or 6 within the hexamer. The L273D mutation inhibits STM1 binding to the Orail C-terminus (7) and would be expected to reduce the current amplitude by an amount dependent on the number of mutations in the channel. mCh-STM1 and GFP-tagged 6xOrail were coexpressed in HEK293 cells, and before recording, GFP and

mCherry fluorescence was measured at the cell perimeter to ensure that STIM1 expression was not limiting for channel activity (see [Materials and Methods](#)). Similar to native CRAC channels, 6xOrai1 channels produced inward currents that developed slowly over tens of seconds after break-in, due to passive ER  $\text{Ca}^{2+}$  depletion elicited by EGTA in the recording pipette ([Fig. 2 A](#)). We found that regardless of its position in the hexamer (subunit 1, 3, or 6), the L273D mutation inhibited the maximum steady-state current to the same degree ( $\sim 2/3$ ) relative to currents carried by the wild-type (WT) 6xOrai1 ([Fig. 2 B](#);  $p = 0.0045$ , significant between WT and L273D; not significant among L273D variants using analysis of variance). The reduced current levels in the three mutant channels were not the result of reduced expression; WT and mutant hexamers were all expressed at equivalent levels at the plasma membrane as assessed by staining with 2C1.1, a monoclonal antibody that specifically binds the extracellular III-IV loop of human Orai1 ([34](#)) ([Fig. S1](#)). CDI also varies with the degree

of STIM1 binding to Orai1 ([21,22,25](#)), providing an additional test of subunit incorporation that is independent of expression level. Like the current amplitude, the extent of inactivation was reduced to a similar degree for the three mutant 6xOrai1 constructs relative to WT 6xOrai1 ([Fig. 2, C and D](#); not significant among L273D variants at all test potentials using analysis of variance). Thus, the effects of L273D on activation and inactivation indicate that each subunit in the hexamer participates equally in forming functional channels. Combining the biochemical and electrophysiological data, we therefore conclude that each channel in the plasma membrane functions as a hexamer of Orai1 subunits.

### Orai1 hexamers display the characteristic properties of CRAC channels

Given that the 6xOrai1 construct produces functional hexameric channels, we next considered whether the

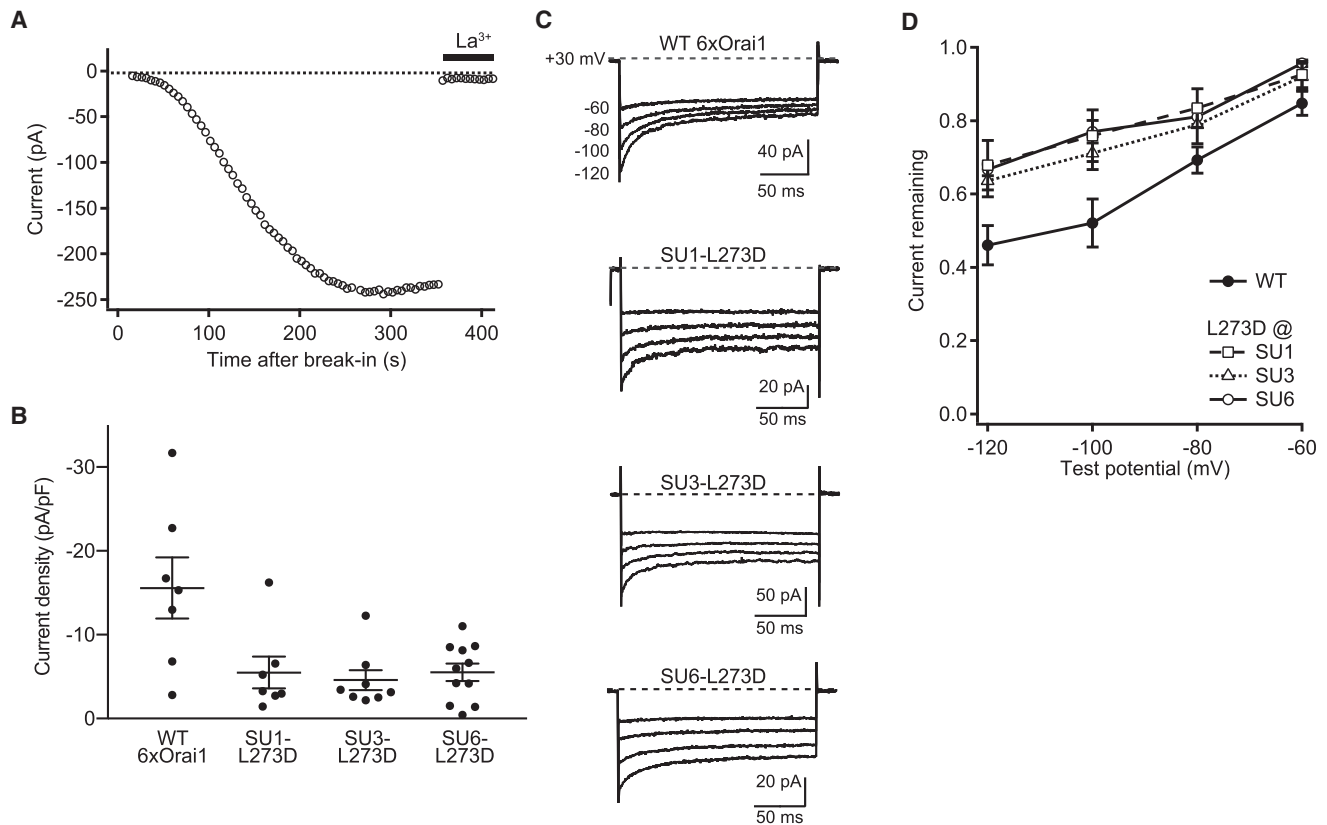


**FIGURE 2** All subunits of the Orai1 hexamer contribute equally to channel gating. Whole-cell currents were recorded in the presence of 20 mM extracellular  $\text{Ca}^{2+}$  ( $\text{Ca}^{2+}_o$ ) from HEK293 cells transfected with mCh-STIM1 and 6xOrai1-GFP. (A) Wild-type 6xOrai1 current at  $-100$  mV developed slowly after break-in with 10 mM EGTA in the recording pipette and was blocked by addition of 10  $\mu\text{M}$   $\text{La}^{3+}$ . (B) Reduction of channel activity by L273D mutations introduced into the indicated subunit (SU) of the hexamer. Channel activity is plotted as the peak CRAC current density at  $-100$  mV (circles, individual cells; lines, mean  $\pm$  SE;  $n = 7$ –11 cells per hexamer variant). (C) Effects of single L273D mutations on the extent of CDI. CDI was evoked by 200-ms steps from the holding potential of  $+30$  mV to the indicated test potentials. The L273D mutation in each of three indicated subunits reduced the extent of CDI relative to the WT hexamer. (D) The extent of CDI plotted as a function of voltage for WT and L273D mutant hexamers, and quantified as current remaining at the end of the step relative to the peak current (see [Materials and Methods](#)). The L273D mutation reduced CDI similarly regardless of its location in subunit 1, 3, or 6, across the entire voltage range (mean  $\pm$  SE,  $n = 4$ –6 cells per hexamer variant).

channels exhibit characteristic CRAC channel properties by comparing currents in cells expressing 1xOrai1 and 6xOrai1. Previous work has shown that channels made from monomeric hOrai1 constructs generate currents that are highly similar to endogenous CRAC channels (2). We assessed a comprehensive set of characteristics, including ion selectivity, CDI, sensitivity to 2-aminoethoxydiphenyl borate (2-APB),  $\text{Ca}^{2+}$  binding affinity, unitary conductance, and open probability.

#### Ion selectivity

CRAC channels are extremely  $\text{Ca}^{2+}$  selective, with pronounced inward rectification and a reversal potential  $>+50$  mV in the presence of extracellular  $\text{Ca}^{2+}$  ( $\text{Ca}^{2+}_o$ ) (2). The current-voltage relations of 6xOrai1 and 1xOrai1 channels in 20 mM  $\text{Ca}^{2+}_o$  were indistinguishable with reversal potentials  $>+50$  mV (Fig. 3 A), consistent with a high  $\text{Ca}^{2+}$  selectivity. Replacement of extracellular  $\text{Na}^+$  with the large cation NMDG did not reduce the current produced by 6xOrai1 channels, confirming that the current is carried entirely by  $\text{Ca}^{2+}$  (data not shown). In the absence of divalent cations,  $\text{Ca}^{2+}$  no longer occupies the selectivity filter of CRAC channels, allowing monovalent cations to permeate (26,35,36). Under divalent-free (DVF) conditions the I/V relations for 6xOrai1 and 1xOrai1 currents were indistinguishable, with reversal potentials of  $45.8 \pm 1.2$  mV (6xOrai1, four cells) and  $46.8 \pm 0.6$  mV (1xOrai1, four cells), corresponding to a  $P_{\text{Cs}}/P_{\text{Na}}$  ratio of 0.16 (Fig. 3 B). These results demonstrate that the ionic selectivity of the Orai1 hexamer for  $\text{Ca}^{2+}$  and  $\text{Na}^+$  matches that of the CRAC channel.

#### Rapid $\text{Ca}^{2+}$ -dependent inactivation

Local accumulation of intracellular  $\text{Ca}^{2+}$  near the CRAC channel pore feeds back to inhibit current over a timescale of tens of milliseconds (37,38). CDI was evoked by 200-ms hyperpolarizing voltage pulses in the range of  $-60$  to  $-120$  mV (Fig. 4 A). The 6xOrai1 and 1xOrai1 channels inactivated to the same extent over this voltage range (Fig. 4 B). In addition, CDI for the 6xOrai1 and 1xOrai1 channels followed a biexponential time course with comparable fast and slow time constants and amplitudes (Fig. 4, C and D). Thus, 6xOrai1 channels display the same inactivation gating behavior as channels made from unlinked Orai1, which is similar to that of native CRAC channels.

#### Biphasic effects of 2-APB

2-APB enhances CRAC current at low doses (1–5  $\mu\text{M}$ ) and causes transient enhancement followed by inhibition at higher doses ( $\geq 10$   $\mu\text{M}$ ) (21,39). When applied at low and high doses, 2-APB evoked similar degrees of current enhancement and inhibition in cells expressing 6xOrai1 and 1xOrai1 channels (Fig. 5).

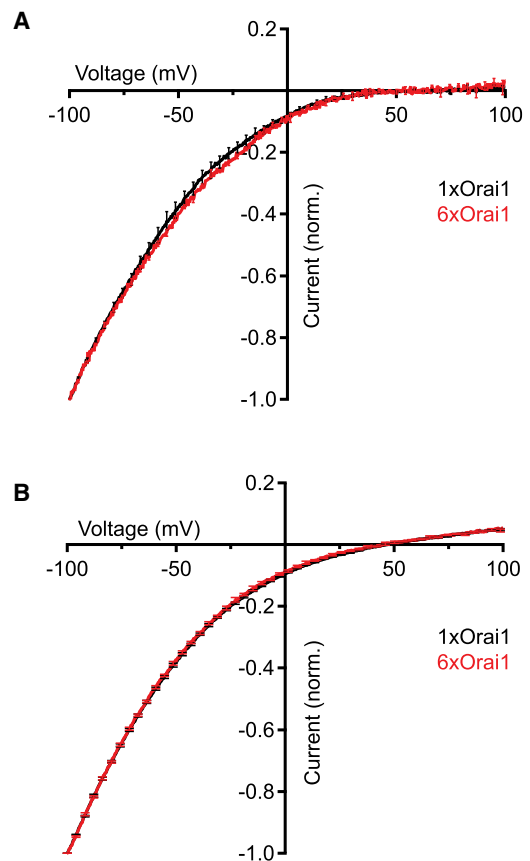


**FIGURE 3** Ion selectivity of hexameric Orai1 concatemers. After whole-cell currents reached steady state, I/V relations were collected in response to voltage ramps from  $-100$  to  $+100$  mV. (A) The average I/V relations in the presence of 20 mM  $\text{Ca}^{2+}_o$  are similar for 6xOrai1 (red) and 1xOrai1 channels (black). To facilitate comparisons, currents in (A) and (B) were normalized to their value at  $-100$  mV before averaging ( $n = 4$  cells). Mean  $\pm$  SE is displayed for every 10th point. (B) Under DVF conditions that allow monovalent cations to permeate, the I/V relations of the 6xOrai1 (red) and 1xOrai1 channels (black) are identical. Ramp currents from four cells were recorded within 3–10 s after DVF was applied, averaged, and plotted on a normalized scale as in (A). To see this figure in color, go online.

#### $\text{Ca}^{2+}$ block of monovalent permeation

The extremely small conductance of CRAC channels precludes the use of single-channel recording to determine directly the unitary conductance and open probability ( $P_o$ ). However, these elementary channel properties may be estimated from ensemble current noise measurements, based on the ability of micromolar  $\text{Ca}^{2+}$  to reversibly bind to the selectivity filter and transiently inhibit  $\text{Na}^+$  flux, creating current fluctuations and reducing the overall open probability of the channel (26). After induction of CRAC current in the presence of  $\text{Ca}^{2+}$ , divalent-free solution was applied to allow  $\text{Na}^+$  conduction, manifest as a large current increase followed by a slow decline due to channel depotentiation (26,35,40) (Fig. 6 A). The peak current was taken to indicate the maximal  $\text{Na}^+$  current level, while various concentrations of  $\text{Ca}^{2+}$  were added to the DVF solution to reduce the peak

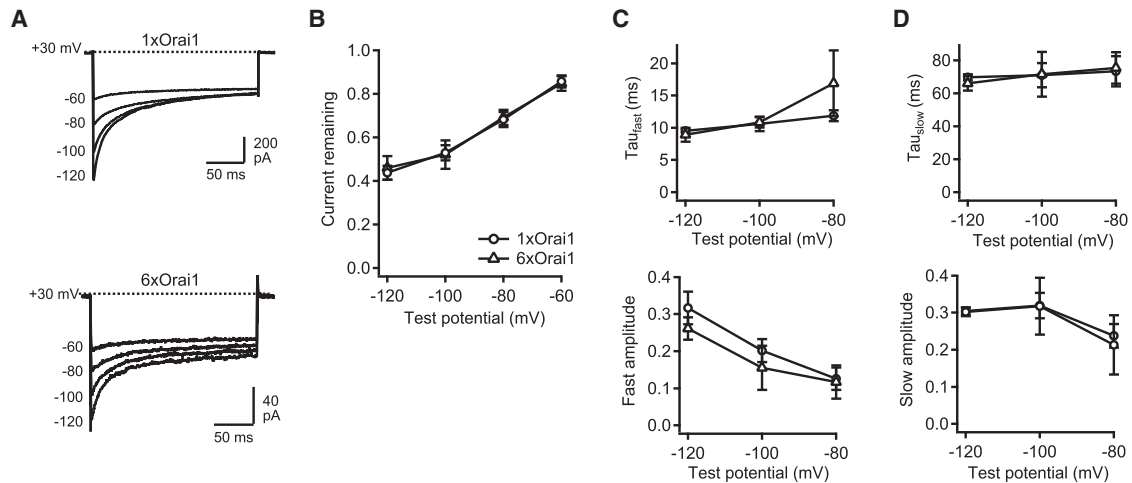


FIGURE 4  $\text{Ca}^{2+}$ -dependent inactivation of hexameric Orai1 concatemers. (A) Inactivating currents evoked in 20 mM  $\text{Ca}^{2+}_o$  by hyperpolarizing pulses to the indicated potentials in two cells coexpressing mCh-*STIM1* with 6xOrai1 or 1xOrai1 constructs. (B) The extent of CDI is identical for 6xOrai1 and 1xOrai1 channels over a wide voltage range. In (B–D), mean  $\pm$  SE values ( $n = 4$  cells) are shown from cells expressing 6xOrai1 ( $\Delta$ ) and 1xOrai1 channels ( $\circ$ ). (C and D) Time constants (*top*) and amplitudes (*bottom*) from a biexponential function ( $I = I_0 + A_1e^{-t/\tau_1} + A_2e^{-t/\tau_2}$ ) fitted to the current time course for each hyperpolarization in (A). Fast and slow time constants and amplitudes are not significantly different for 6xOrai1 and 1xOrai1 channels.

$\text{Na}^+$  current and measure  $\text{Ca}^{2+}$  block affinity.  $\text{Ca}^{2+}$  blocked  $\text{Na}^+$  current through the 6xOrai1 channel pore with the same affinity and Hill coefficient as seen for 1xOrai1 channels (Fig. 6 C; Table 1), suggesting that the  $\text{Ca}^{2+}$  binding site in channels made from 6xOrai1 DNA closely resembles that of native CRAC channels and channels made from 1xOrai1 DNA.

#### Open probability and unitary conductance

Current variance was measured during 200-ms sweeps collected during the peak  $\text{Na}^+$  current after each solution exchange (Fig. 6 B). Fig. 6 D shows examples of the parabolic relationship of variance to current in two cells, indicating  $P_o$  values of 0.82 and 0.74 and unitary currents of  $-87$  fA and  $-91$  fA at  $-100$  mV for 6xOrai1 and 1xOrai1, respectively. The mean  $P_o$  and unitary current amplitudes of 1xOrai1 and 6xOrai1 channels from several cells are shown in Table 1 and compared to values reported for endogenous CRAC channels in Jurkat T lymphocytes (26). The results show that the Orai1 hexamer reproduces elementary channel properties of the CRAC channel, including the characteristic low unitary conductance and high open probability.

## DISCUSSION

The subunit stoichiometry of the CRAC channel is currently unresolved, with conflicting evidence for Orai1 tetramers and hexamers based on biochemical and structural approaches. Here we have characterized a concatenated hexamer of Orai1 and show that it reproduces the unique biophysical characteristics of the CRAC channel, including ion selectivity, activation and inactivation gating, and unitary current and open probability. These results offer strong

functional evidence to support the hexameric CRAC channel stoichiometry described by the dOrai crystal structure (13).

### Assembly of channels from hexameric Orai1 concatemers

Our conclusion regarding CRAC channel stoichiometry rests on evidence that functional channels form from the complete hexameric construct. Thus, it is important to consider several problems known to cause improper assembly of concatemers. First, partial polypeptide synthesis occurring through mRNA degradation, premature termination of translation, or proteolysis can generate polypeptides with only a subset of concatemer subunits, which may then recombine to form channels. This issue was described in a study of trimeric P2X<sub>1</sub> channels, in which functional channels in the plasma membrane formed from monomer and dimer byproducts whereas full-length protein was found to be trapped in intracellular aggregates (29). In whole-cell lysates it can be difficult to detect partial protein products at the plasma membrane against a much higher background of aggregated intracellular protein; thus, surface biotinylation is key for specifically characterizing the plasma membrane fraction (29). In our experiments, the majority of 6xOrai1 protein appeared to be intracellular, possibly reflecting aggregated or misfolded protein. However, biotinylated plasma membrane proteins displayed the expected size of the full Orai1 hexamer, without significant amounts of smaller fragments. Thus, we conclude that the channel activity we record is derived from full-length 6xOrai1 polypeptides.

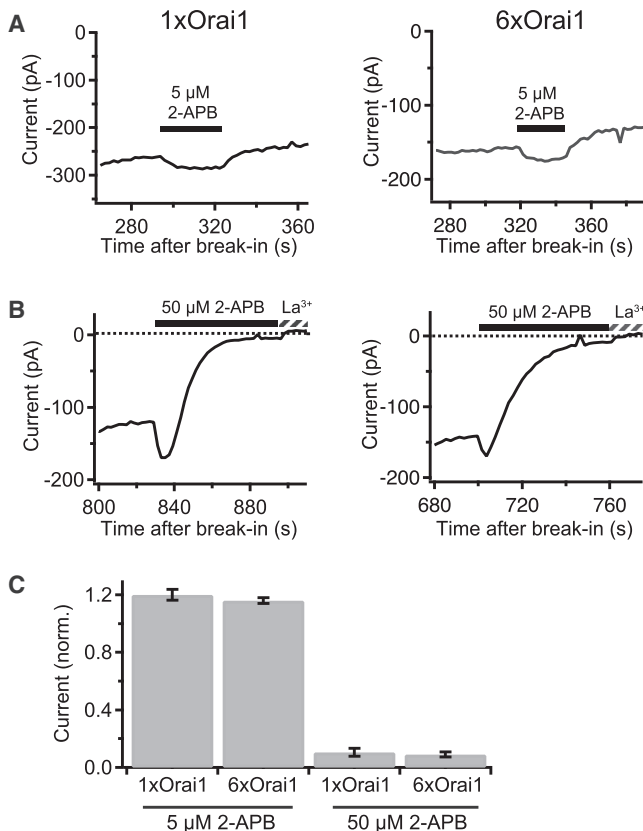


**FIGURE 5** Enhancement and inhibition of hexameric Orai1 concatemers by 2-APB. (A) 5  $\mu\text{M}$  2-APB enhances steady-state  $\text{Ca}^{2+}$  current through 1xOrai1 (left) or 6xOrai1 channels (right). Currents are from two cells at  $-100$  mV in 20 mM  $\text{Ca}^{2+}_o$ . (B) A higher dose of 2-APB (50  $\mu\text{M}$ ) transiently enhances and stably inhibits currents through 1xOrai1 (left) and 6xOrai1 channels (right). 100  $\mu\text{M}$   $\text{La}^{3+}$  was added as indicated to fully block current. (C) Summary of the effects of 2-APB. Enhancement and inhibition of current are normalized to the current magnitude immediately before application of the drug. Averages are mean  $\pm$  SE,  $n = 4$ –7 cells.

Despite the presence of full-length hexameric protein in the plasma membrane, another potential complication is that only a subset of subunits might assemble to form channels (33), raising the possibility that 6xOrai constructs could form tetrameric channels. In addition, subunits from multiple polypeptides could combine with each other, so that the assembled protein would fail to reproduce the number and locations of mutations in the concatemer. Because the L273D mutation reduced both channel activity and the extent of CDI by the same amounts regardless of its position in subunits 1, 3, or 6, it appears that each of the six subunits contributes equally to the channel. The simplest scenario consistent with this result is that each channel assembles as a hexamer from a single polypeptide. While it is possible that a subset of subunits could form a tetramer, or subunits from separate 6xOrai1 polypeptides combine to form a hexameric channel, each concatemeric subunit would have to incorporate with equal probability. Previous studies have shown that subunit usage is biased in cases

where only a subset of concatemeric subunits assemble to form a channel, with N-terminal subunits incorporating more efficiently; examples include tetrameric Kv1.1 channels made from pentameric concatemer DNA (33) and trimeric P2X<sub>2</sub> receptors made from tandem tetramer or hexamer constructs (41). Thus, our observations of equal subunit incorporation strongly suggest that the channel stoichiometry is not less than six. Equal usage of concatemeric subunits also argues against the possibility that multiple polypeptides contribute subunits to a single hexameric channel, considering that the high local concentration of subunits within a single polypeptide would be expected to favor coupling between contiguous subunits and thereby bias subunit usage. Thus, the equal contributions of subunits 1, 3, and 6 we have observed would not be expected if channels were formed from a subset of subunits or from multiple polypeptides. For this reason, we conclude that the channels likely formed from single full-length hexameric polypeptides.

### Hexameric Orai1 channels display the biophysical fingerprint of native CRAC channels

Several lines of evidence show that Orai1 hexamers display the same activation and inactivation gating properties as unlinked (native or overexpressed) CRAC channels. First, 6xOrai1 current developed gradually in response to passive ER store depletion, consistent with STIM1-dependent activation. Upon maximal activation, 6xOrai1 channels displayed a high open probability similar to Jurkat CRAC channels (26), implying that STIM1 binding activates 6xOrai1 and native CRAC channels to the same high- $P_o$  state. Second, 2-APB modulated 6xOrai1 and 1xOrai1 currents similarly. While 2-APB mechanisms are not well understood, the enhancement and inhibition of current are thought to reflect changes in STIM1 binding to Orai1 or the coupling of STIM1 binding to CRAC channel opening (42–44). Thus, the similar effects of 2-APB on 6xOrai1 and 1xOrai1 currents are consistent with a shared activation gating mechanism. Finally, 6xOrai1 channels inactivate to a similar extent and with the same kinetics as unlinked channels, indicating that they share a common inactivation mechanism. The mechanism of CDI is still unclear, but the concerted action of the inactivation domain of STIM1 ( $ID_{\text{STIM}}$ ) and Orai1 inner pore residue W76 control its extent while the pore residue Y80 modulates CDI kinetics (24). Activation and inactivation gating are both sensitive to the STIM1 binding stoichiometry (7,21,22,25). That these processes are normal in 6xOrai1 channels suggests that linking Orai1 subunits together does not negatively impact STIM1 binding to the Orai1 C-termini to cause channel opening, nor does it prevent  $ID_{\text{STIM}}$  from acting with the Orai1 N-terminus to drive inactivation. We cannot rule out subtle binding or allosteric changes caused by linking Orai1 subunits, but if such changes do occur, they should

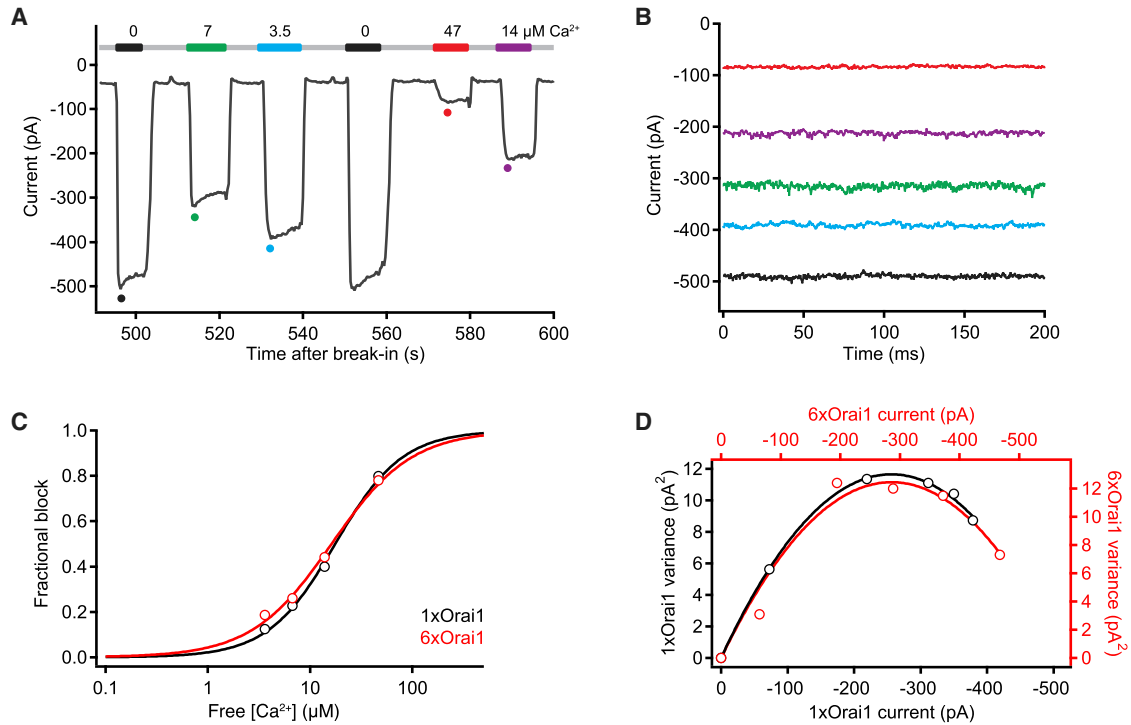


**FIGURE 6** Ensemble variance analysis of hexameric Orai1 concatemers. (A) A thapsigargin-pretreated cell coexpressing 6xOrai1 and mCh-STIM1 was transiently exposed to a series of DVF solutions containing various amounts of free  $\text{Ca}^{2+}$  to partially block monovalent current. Current at a holding potential of  $-100$  mV is displayed, with the gray line indicating  $2$  mM  $\text{Ca}^{2+}_o$  and colored bars indicating DVF with added  $\text{Ca}^{2+}$ . (B) 200-ms current sweeps collected at the times indicated by the colored dots in (A). Current variance increases and then declines in response to increasing block by  $\text{Ca}^{2+}$ . (C)  $\text{Ca}^{2+}$ -dependent block of  $\text{Na}^+$  current in two cells expressing 1xOrai1 (black) or 6xOrai1 (red). Curves represent best fits of the Hill equation,  $\text{block} = 1/[1 + (K_{1/2}/[\text{Ca}])^{n_H}]$ , with  $K_{1/2} = 17.6$   $\mu\text{M}$  and  $n_H = 1.3$  (1xOrai1), or  $K_{1/2} = 16.2$   $\mu\text{M}$  and  $n_H = 1.1$  (6xOrai1). (D) Plots of baseline-corrected current variance versus amplitude in two cells expressing 1xOrai1 (black) or 6xOrai1 (red) and exposed to DVF with partially blocking  $\text{Ca}^{2+}$  concentrations. Parabolic fits indicate the unitary current amplitude ( $-87$  fA for 6xOrai1,  $-91$  fA for 1xOrai1) and channel open probability in the absence of  $\text{Ca}^{2+}$  ( $P_o = 0.82$  for 6xOrai1,  $0.74$  for 1xOrai1) (see [Materials and Methods](#)). To see this figure in color, go online.

be obviated by cleaving the intersubunit linkers with TEV protease.

Orai1 hexamers also possess a permeation pathway that is functionally similar to that of unlinked Orai1 or native CRAC channels. Like CRAC channels, 6xOrai1 channels in the presence of extracellular  $\text{Ca}^{2+}$  are inwardly rectifying, lack a clearly defined reversal potential ( $>+50$  mV), and are completely blocked by  $10$   $\mu\text{M}$   $\text{La}^{3+}$ .  $\text{Ca}^{2+}$  blocks monovalent cation permeation through 6xOrai1, 1xOrai1, and CRAC channels with the same affinity (Table 1). In the absence of divalent cations, the

6xOrai1 channels and unlinked channels show the same low permeability of  $\text{Cs}^+$  relative to  $\text{Na}^+$ , and their  $\text{Na}^+$  flux rates as indicated by unitary current amplitudes are also similar. It is important to note that the pore properties of  $\text{Ca}^{2+}$  block affinity, ion selectivity, and unitary conductance are sensitive to the precise geometry of the selectivity filter and other flux-limiting regions of the permeation pathway. Thus, it is highly unlikely that these permeation properties would be identical for tetrameric and hexameric arrangements of Orai1 pore subunits. Therefore, the shared permeation properties of 6xOrai1 and native CRAC

**TABLE 1** Unitary Properties of Native CRAC Channels and Channels Derived from 1xOrai1 or 6xOrai1

Channel	$P_o$	$i_{\text{Na}}$ (fA)	$\text{Ca}^{2+}$ Affinity ( $K_{1/2}$ , $\mu\text{M}$ )	$n_H$	$n$
Native CRAC <sup>a</sup>	$0.79 \pm 0.02$	$-90.9^b$	19.6	1.2	3–10
1xOrai1 <sup>b</sup>	$0.81 \pm 0.04$	$-89.5 \pm 1.5$	$16.4 \pm 1.2$	$1.33 \pm 0.08$	3
6xOrai1 <sup>b</sup>	$0.76 \pm 0.04$	$-86.9 \pm 7.0$	$15.9 \pm 2.7$	$1.15 \pm 0.02$	4

Values are mean  $\pm$  SE. For all properties,  $p > 0.05$  between 1xOrai1 and 6xOrai1 using a two-tailed  $t$ -test.

<sup>a</sup>Data from Jurkat cell  $I_{\text{CRAC}}$  measured at  $-110$  mV, taken from Prakriya and Lewis (26). The  $i_{\text{Na}}$  value here is extrapolated to a potential of  $-100$  mV using the  $\text{Na}^+ - I_{\text{CRAC}}$   $I/V$  relation.

<sup>b</sup>1xOrai1 and 6xOrai1 channel properties measured at  $-100$  mV.

channels strongly suggest that the native CRAC channel functions as a hexamer of Orai1 subunits.

### Comparisons with previous work

Our observations that hexameric Orai1 channels have hallmark CRAC channel properties conflict with a previous report in which a concatemeric hexamer of Orai1 displayed significantly reduced  $\text{Ca}^{2+}$  selectivity and completely lacked CDI (17). One potentially significant difference between the two studies is our use of longer linkers (24 vs. 6 amino acids in the earlier study). A study of pentameric GABA<sub>A</sub> receptor concatemers showed that linkers below a critical length reduced channel activity and apparent GABA binding affinity (27). Further tests will be needed to determine the impact of linker length on the properties of concatemeric Orai1 channels, and whether this can explain the difference between the two studies.

Previous results supporting a tetrameric stoichiometry for the CRAC channel contrast with our evidence in favor of hexamers. Interestingly, single-molecule photobleaching experiments have provided evidence for multiple Orai1 stoichiometries at the plasma membrane. While one study reported that PM Orai1 is exclusively tetrameric in resting cells (5), two others concluded that PM Orai1 is mostly dimeric in the resting state, but rearranges into higher-order multimers following store depletion in the presence of STIM1 (10,12). These multimers may encompass a mixture of dimers, tetramers and hexamers (12), although the stochastic and flickery nature of GFP fluorescence precludes a precise assignment. Thus, several studies support the possibility of multiple Orai1 protein stoichiometries in the plasma membrane; however, because single-molecule measurements require extremely low expression levels, function is not easily assigned to any particular stoichiometry.

Functional evidence for tetrameric Orai1 channels has instead been derived from cells overexpressing a tetrameric Orai1 DNA. Coexpression of a dominant negative Orai1 E106Q monomer DNA failed to inhibit current from Orai1 tetrameric concatemer, suggesting that the tetrameric polypeptides do not combine to form higher-order multimers (6). However, it is difficult to exclude the possibility that at high expression levels, multiple tetramers may preferentially combine to form hexamers rather than incorporate exogenous monomeric subunits. A definitive description of channel assembly from tetrameric concatemers is beyond the scope of this study, but may be approachable using a biochemical method such as crosslinking of cysteines introduced at subunit interfaces, as has been applied to determine subunit arrangements in other channels (45). Importantly, our finding that hexameric Orai1 channels share the detailed pore properties of the CRAC channel strongly implies that the native CRAC channel has the same pore geometry as the Orai1 hexamer, and hence is likely to function as a hexamer rather than a tetramer.

Others have suggested the possibility that the *Drosophila* Orai stoichiometry reported by Hou et al. (13) might differ from that of native human Orai1 because of species differences, mutations and truncations that were introduced to allow crystallization, and the use of detergents that have the capacity to alter channel stoichiometry (4,17) as has been documented for the *S. aureus* MscL channel (46). While the reconstituted dOrai protein with an activating pore mutation did flux  $\text{Na}^{+}$  (13), it was not clear from this result alone whether the hexamer faithfully reproduces a definitive set of CRAC channel properties. Thus, our observations that hexameric CRAC channels are biophysically identical to native CRAC channels provide essential functional evidence to support the hexameric dOrai crystal structure (13). In addition, these results validate the use of the hexameric Orai1 concatemer as an important experimental tool for dissecting the roles of individual subunits and cooperative interactions in the control of CRAC channel gating and permeation.

### SUPPORTING MATERIAL

One figure and two tables are available at [http://www.biophysj.org/biophysj/supplemental/S0006-3495\(16\)30820-7](http://www.biophysj.org/biophysj/supplemental/S0006-3495(16)30820-7).

### AUTHOR CONTRIBUTIONS

M.Y., L.A.L., and R.S.L. designed research and analyzed data; M.Y. and L.A.L. performed research; and M.Y. and R.S.L. wrote the article.

### ACKNOWLEDGMENTS

We thank Minnie Wu for experimental advice, Anshul Rana for constructive feedback, and the Lewis Lab for comments on the article. We are grateful to Tao Xu for supplying the Orai-GFP plasmid and Helen McBride for providing us with 2C1.1 mAb. Flow cytometry was performed in the Stanford Shared FACS Facility, and we thank Cathy Crumpton for flow cytometry operator support.

This work was funded by National Institutes of Health award No. R37GM45374 and the Mathers Charitable Foundation (to R.S.L.). M.Y.'s training was supported by the National Science Foundation Graduate Research Fellowship Program, the Stanford Masters of Medicine Program, and National Institutes of Health training grant No. 5T32AI007290 to the Stanford Immunology Graduate Program.

### REFERENCES

- Hogan, P. G., R. S. Lewis, and A. Rao. 2010. Molecular basis of calcium signaling in lymphocytes: STIM and ORAI. *Annu. Rev. Immunol.* 28:491–533.
- Prakriya, M., and R. S. Lewis. 2015. Store-operated calcium channels. *Physiol. Rev.* 95:1383–1436.
- Amcheslavsky, A., M. L. Wood, ..., M. D. Cahalan. 2015. Molecular biophysics of Orai store-operated  $\text{Ca}^{2+}$  channels. *Biophys. J.* 108:237–246.
- Chen, L., and T. Xu. 2013. On the stoichiometry of resting and activated CRAC channels. *Curr. Top. Membr.* 71:95–108.

5. Ji, W., P. Xu, ..., L. Chen. 2008. Functional stoichiometry of the unitary calcium-release-activated calcium channel. *Proc. Natl. Acad. Sci. USA*. 105:13668–13673.
6. Mignen, O., J. L. Thompson, and T. J. Shuttleworth. 2008. Orai1 subunit stoichiometry of the mammalian CRAC channel pore. *J. Physiol.* 586:419–425.
7. Li, Z., L. Liu, ..., T. Xu. 2011. Graded activation of CRAC channel by binding of different numbers of STIM1 to Orai1 subunits. *Cell Res.* 21:305–315.
8. Thompson, J. L., O. Mignen, and T. J. Shuttleworth. 2009. The Orai1 severe combined immune deficiency mutation and calcium release-activated  $\text{Ca}^{2+}$  channel function in the heterozygous condition. *J. Biol. Chem.* 284:6620–6626.
9. Madl, J., J. Weghuber, ..., G. J. Schütz. 2010. Resting state Orai1 diffuses as homotrimer in the plasma membrane of live mammalian cells. *J. Biol. Chem.* 285:41135–41142.
10. Penna, A., A. Demuro, ..., M. D. Cahalan. 2008. The CRAC channel consists of a tetramer formed by Stim-induced dimerization of Orai dimers. *Nature*. 456:116–120.
11. Demuro, A., A. Penna, ..., I. Parker. 2011. Subunit stoichiometry of human Orai1 and Orai3 channels in closed and open states. *Proc. Natl. Acad. Sci. USA*. 108:17832–17837.
12. Li, P., Y. Miao, ..., M. Vig. 2016.  $\alpha$ -SNAP regulates dynamic, on-site assembly and calcium selectivity of Orai1 channels. *Mol. Biol. Cell*. 27:2542–2553.
13. Hou, X., L. Pedi, ..., S. B. Long. 2012. Crystal structure of the calcium release-activated calcium channel Orai. *Science*. 338:1308–1313.
14. Balasuriya, D., S. Srivats, ..., J. M. Edwardson. 2014. Atomic force microscopy (AFM) imaging suggests that stromal interaction molecule 1 (STIM1) binds to Orai1 with sixfold symmetry. *FEBS Lett.* 588:2874–2880.
15. Zhou, Y., S. Ramachandran, ..., P. G. Hogan. 2010. Pore architecture of the ORAI1 store-operated calcium channel. *Proc. Natl. Acad. Sci. USA*. 107:4896–4901.
16. McNally, B. A., M. Yamashita, ..., M. Prakriya. 2009. Structural determinants of ion permeation in CRAC channels. *Proc. Natl. Acad. Sci. USA*. 106:22516–22521.
17. Thompson, J. L., and T. J. Shuttleworth. 2013. How many Orai's does it take to make a CRAC channel? *Sci. Rep.* 3:1961.
18. Wu, M. M., J. Buchanan, ..., R. S. Lewis. 2006.  $\text{Ca}^{2+}$  store depletion causes STIM1 to accumulate in ER regions closely associated with the plasma membrane. *J. Cell Biol.* 174:803–813.
19. Li, Z., J. Lu, ..., T. Xu. 2007. Mapping the interacting domains of STIM1 and Orai1 in  $\text{Ca}^{2+}$  release-activated  $\text{Ca}^{2+}$  channel activation. *J. Biol. Chem.* 282:29448–29456.
20. Bers, D. M., C. W. Patton, and R. Nuccitelli. 2010. A practical guide to the preparation of  $\text{Ca}^{2+}$  buffers. *Methods Cell Biol.* 99:1–26.
21. Scrimgeour, N., T. Litjens, ..., G. Y. Rychkov. 2009. Properties of Orai1 mediated store-operated current depend on the expression levels of STIM1 and Orai1 proteins. *J. Physiol.* 587:2903–2918.
22. Hoover, P. J., and R. S. Lewis. 2011. Stoichiometric requirements for trapping and gating of  $\text{Ca}^{2+}$  release-activated  $\text{Ca}^{2+}$  (CRAC) channels by stromal interaction molecule 1 (STIM1). *Proc. Natl. Acad. Sci. USA*. 108:13299–13304.
23. Mullins, F. M., M. Yen, and R. S. Lewis. 2016. Orai1 pore residues control CRAC channel inactivation independently of calmodulin. *J. Gen. Physiol.* 147:137–152.
24. Mullins, F. M., and R. S. Lewis. 2016. The inactivation domain of STIM1 is functionally coupled with the Orai1 pore to enable  $\text{Ca}^{2+}$ -dependent inactivation. *J. Gen. Physiol.* 147:153–164.
25. McNally, B. A., A. Somasundaram, ..., M. Prakriya. 2012. Gated regulation of CRAC channel ion selectivity by STIM1. *Nature*. 482:241–245.
26. Prakriya, M., and R. S. Lewis. 2006. Regulation of CRAC channel activity by recruitment of silent channels to a high open-probability gating mode. *J. Gen. Physiol.* 128:373–386.
27. Baumann, S. W., R. Baur, and E. Sigel. 2001. Subunit arrangement of  $\gamma$ -aminobutyric acid type A receptors. *J. Biol. Chem.* 276:36275–36280.
28. Sack, J. T., O. Shamotienko, and J. O. Dolly. 2008. How to validate a heteromeric ion channel drug target: assessing proper expression of concatenated subunits. *J. Gen. Physiol.* 131:415–420.
29. Nicke, A., J. Rettinger, and G. Schmalzing. 2003. Monomeric and dimeric byproducts are the principal functional elements of higher order P2X<sub>1</sub> concatamers. *Mol. Pharmacol.* 63:243–252.
30. McCormack, K., L. Lin, ..., F. J. Sigworth. 1992. Tandem linkage of *Shaker*  $\text{K}^{+}$  channel subunits does not ensure the stoichiometry of expressed channels. *Biophys. J.* 63:1406–1411.
31. Shapiro, M. S., and W. N. Zagotta. 1998. Stoichiometry and arrangement of heteromeric olfactory cyclic nucleotide-gated ion channels. *Proc. Natl. Acad. Sci. USA*. 95:14546–14551.
32. Groot-Kormelink, P. J., S. D. Broadbent, ..., L. G. Sivilotti. 2004. Incomplete incorporation of tandem subunits in recombinant neuronal nicotinic receptors. *J. Gen. Physiol.* 123:697–708.
33. Liman, E. R., J. Tytgat, and P. Hess. 1992. Subunit stoichiometry of a mammalian  $\text{K}^{+}$  channel determined by construction of multimeric cDNAs. *Neuron*. 9:861–871.
34. Lin, F. F., R. Elliott, ..., H. J. McBride. 2013. Generation and characterization of fully human monoclonal antibodies against human Orai1 for autoimmune disease. *J. Pharmacol. Exp. Ther.* 345:225–238.
35. Lepple-Wienhues, A., and M. D. Cahalan. 1996. Conductance and permeation of monovalent cations through depletion-activated  $\text{Ca}^{2+}$  channels ( $I_{\text{CRAC}}$ ) in Jurkat T cells. *Biophys. J.* 71:787–794.
36. Bakowski, D., and A. B. Parekh. 2002. Monovalent cation permeability and  $\text{Ca}^{2+}$  block of the store-operated  $\text{Ca}^{2+}$  current  $I_{\text{CRAC}}$  in rat basophilic leukemia cells. *Pflügers Arch.* 443:892–902.
37. Hoth, M., and R. Penner. 1993. Calcium release-activated calcium current in rat mast cells. *J. Physiol.* 465:359–386.
38. Zweifach, A., and R. S. Lewis. 1995. Rapid inactivation of depletion-activated calcium current ( $I_{\text{CRAC}}$ ) due to local calcium feedback. *J. Gen. Physiol.* 105:209–226.
39. Prakriya, M., and R. S. Lewis. 2001. Potentiation and inhibition of  $\text{Ca}^{2+}$  release-activated  $\text{Ca}^{2+}$  channels by 2-aminoethylidiphenyl borate (2-APB) occurs independently of IP<sub>3</sub> receptors. *J. Physiol.* 536:3–19.
40. Zweifach, A., and R. S. Lewis. 1996. Calcium-dependent potentiation of store-operated calcium channels in T lymphocytes. *J. Gen. Physiol.* 107:597–610.
41. Stoop, R., S. Thomas, ..., R. A. North. 1999. Contribution of individual subunits to the multimeric P2X<sub>2</sub> receptor: estimates based on methanethiosulfonate block at T336C. *Mol. Pharmacol.* 56:973–981.
42. Navarro-Borelly, L., A. Somasundaram, ..., M. Prakriya. 2008. STIM1-Orai1 interactions and Orai1 conformational changes revealed by live-cell FRET microscopy. *J. Physiol.* 586:5383–5401.
43. Wang, Y., X. Deng, ..., D. L. Gill. 2009. STIM protein coupling in the activation of Orai channels. *Proc. Natl. Acad. Sci. USA*. 106:7391–7396.
44. DeHaven, W. I., J. T. Smyth, ..., J. W. Putney, Jr. 2008. Complex actions of 2-aminoethylidiphenyl borate on store-operated calcium entry. *J. Biol. Chem.* 283:19265–19273.
45. Lee, S.-Y., J. A. Letts, and R. MacKinnon. 2008. Dimeric subunit stoichiometry of the human voltage-dependent proton channel Hv1. *Proc. Natl. Acad. Sci. USA*. 105:7692–7695.
46. Dorwart, M. R., R. Wray, ..., P. Blount. 2010. *S. aureus* MscL is a pentamer in vivo but of variable stoichiometries in vitro: implications for detergent-solubilized membrane proteins. *PLoS Biol.* 8:e1000555.

**Biophysical Journal, Volume 111**

**Supplemental Information**

**Functional Analysis of Orai1 Concatemers Supports a Hexameric Stoichiometry for the CRAC Channel**

**Michelle Yen, Ludmila A. Lokteva, and Richard S. Lewis**

## SUPPORTING MATERIAL

### Functional analysis of Orai1 concatemers supports a hexameric stoichiometry for the CRAC channel

Michelle Yen, Ludmila A. Lokteva, and Richard S. Lewis

Department of Molecular and Cellular Physiology, Stanford University School of Medicine, Stanford, CA 94305

**Table S1: PCR primers used to generate Orai1 subunit inserts**

Primer	Purpose	Sequence
1	SU1 for	TCTAAGGCTCGAGGCCACCATGGAGCAAAGCTCATTTCTGAG GA
	SU1 rev	ACGGCAAGCTTGGCATAGTGGCTGCCGGGCGT
2	SU2 for	TAATAAAGCTTGAAAACCTATACTTCCAAGGAGAGCAAAGC TCATTTCTGAGGA
	SU2 rev	ACGGCGAATTCGGCATAGTGGCTGCCGGGCGT
3	SU3 for	AGGAAGAATTCGAGAACCTCTACTTCCAAGGAGAGCAAAGC TCATTTCTGAGGA
	SU3 rev	AGCAAGGTACCGGCATAGTGGCTGCCGGGCGT
4	SU4 for	AGACACGGTACCGAAAACCTATACTTCCAAGGAGAGCAAAG SU4 rev
	SU4 rev	ACGGCGACTGCAGCATAGTGGCTGCCGGGCGTCAG
5	SU5 for	AATAAACTGCAGAAAACCTATACTTCCAAGGAGAGCAAAGC TCATTT
	SU5 rev	TACGGCGATATCGGCATAGTGGCTGCCGGGCGTCAGGG
6	SU6 for	TTACTAGATATCGAAAACCTATACTTCCAAGGAGAGCAAAG SU6 rev
	SU6 rev	ATGCGTGGATCCCATAGTGGCTGCCGGGCGT
7 (SDM)	$\Delta$ Hind for	AGCCGCGCCAAGCTCAAAGCCTCCAGCCG
	$\Delta$ Hind rev	CGGCTGGAGGCTTTGAGCTTGGCGCGGCT
8 (SDM)	TRS for	GGCCCGGGATCCACGAGAACCTTTATTTCCAGGGATCGGTCGC CACCATGGTGAG
	TRS rev	ACCATGGTGGCGACCGATCCCTGGAAATAAAGGTTCTCGTGG ATCCCGGGCCCGC
9 (SDM)	L273D for	ACCGACAGTTCAGGAGGACAACGAGCTGGCGGAG
	L273D rev	CTCCGCCAGCTCGTTGTCCTCCTGGAAGTGTCTCGT

Primer sets were used for PCR amplification except where indicated. Primers used for site-directed mutagenesis are denoted by “SDM”

**Table S2: Linking sequences in the Orai1 concatemeric hexamer**

Orai1 Subunit #	N-term appended sequence	C-term appended sequence
1	XhoI-myc	HindIII
2	HindIII-linker <sup>a</sup>	EcoRI
3	EcoRI-linker <sup>a</sup>	KpnI
4	KpnI-linker <sup>a</sup>	PstI
5	PstI-linker <sup>a</sup>	EcoRV
6	EcoRV-linker <sup>a</sup>	BamHI
C-term eGFP	BamHI-TRS	

<sup>a</sup>linker = TRS (ENLYFQG) + myc (EQKLISEEDL) + Gly-Ser stretch (NGGGGS)

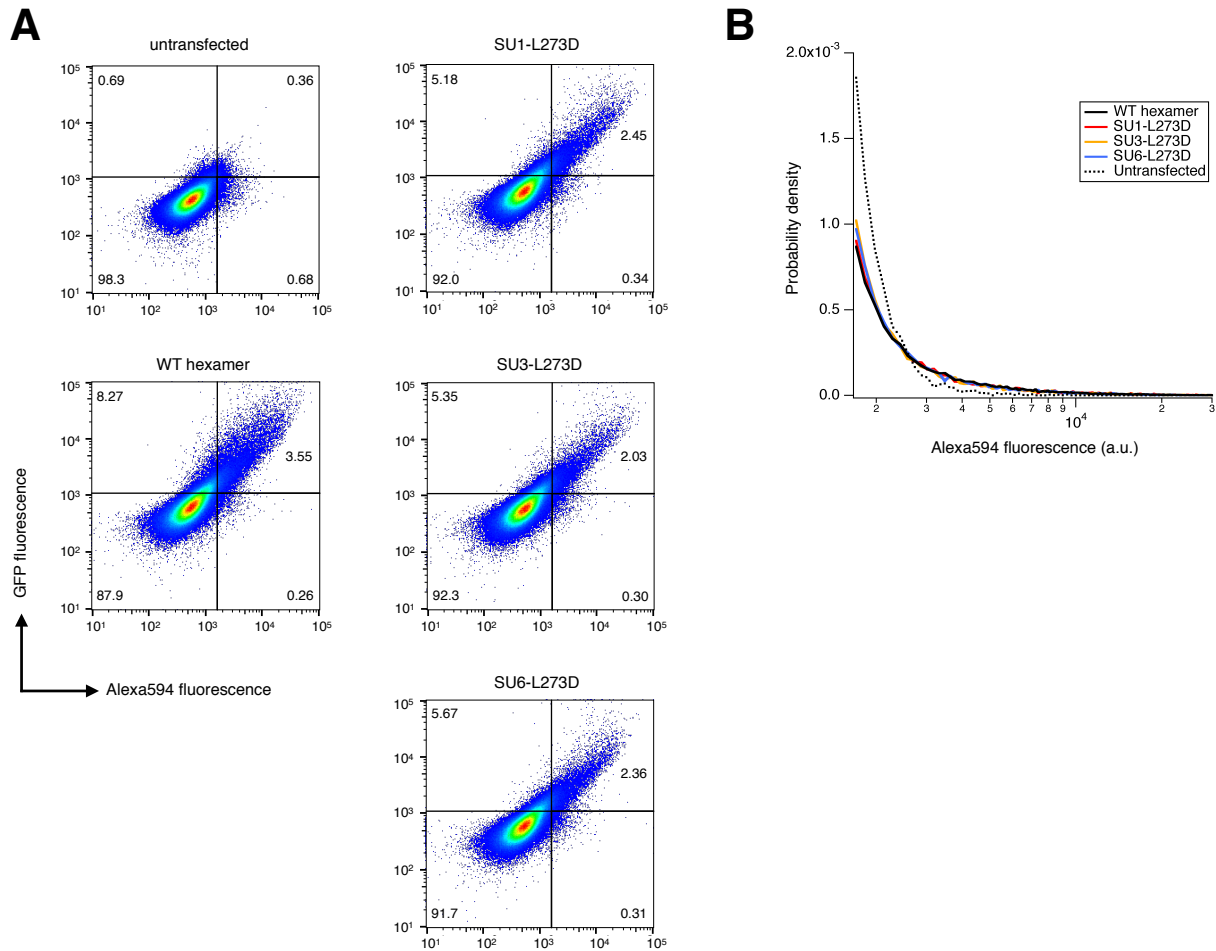


**Figure S1. Flow cytometry analysis of 6xOrai1 expression in the plasma membrane.** (A) Bivariate plot showing GFP (total Orai1) vs 2C1.1-Alexa594 (surface Orai1) fluorescence in untransfected HEK cells and HEK cells transfected with GFP-tagged 6xOrai1 variants. In cells transfected with 6xOrai1-GFP, GFP expression was proportional to Alexa594 fluorescence (upper right quadrants). Untransfected cells stained with 2C1.1 were used to establish a cutoff for GFP and Alexa594 negative and positive populations, as indicated by the quadrant gates. The gates were chosen separately such that 99% of untransfected cells fell in the negative population for GFP and for Alexa594. (B) Histogram of the GFP and Alexa594 double positive population in cells expressing Orai1 hexamer and untransfected cells. The Alexa594 fluorescence distribution is similar between WT and L273D hexamer populations. Each histogram contained > 1000 cells.